Electronic Supplementary Material (ESI) for New Journal of Chemistry.

Supporting information

Competing phenol-imidazole and phenol-phenol interactions in flexible supramolecular environment of N,N'-bis(3-imidazol-1-ylpropyl)naphthalenediimide causing domain expansion

Arup Tarai, Jubaraj B. Baruah*

Physical measurements: Infrared spectra of the solid samples were recorded on a Perkin-Elmer Spectrum-One FT-IR spectrophotometer in the region 4000-400 cm^{-1} by making KBr pellets. Powder X-ray diffraction patterns were recorded using Bruker powder X-ray diffractometer D2 phaser. The ^{1}H-NMR was recorded on a BRUKER Ascend-600 MHz NMR spectrometer using TMS as internal standard. Thermogravimetric analysis (TGA) was performed using a thermal analyzer SDTQ600 simultaneous DTA/TGA system; under nitrogen with a heating rate of 10 °C/min. UV-visible spectra were recorded on a Perkin-Elmer-Lambda 750 UV-vis spectrometer at room temperature. Fluorescence emissions were measured in a Perkin-Elmer LS-55 spectrofluorimeter by taking definite amounts of solutions of samples and exciting at required wavelengths.

Crystallographic Study: X-ray single crystal diffraction data were collected at 298 K with MoKα radiation (λ = 0.71073 Å) on a Bruker Nonius SMART APEX CCD or Oxford SuperNova diffractometer equipped with a graphite monochromator and an Apex CCD camera. SMART software was used for data collection and also for indexing the reflections and determining the unit cell parameters. Data reduction and cell refinement were performed using SAINT and XPREP software. Structures were solved by direct method and refined by full-matrix least-squares on F^2 using SHELXL-2014/7 software or Olex2 1.2-alpha. All non-hydrogen atoms were refined in anisotropic approximation against F^2 of all reflections. Hydrogen atoms of water of hydrated cocrystal **L.phi.H_2O** could not be located by riding model, these were placed at their respective geometric positions, ‘fixed’ and refined in isotropic approximation, other hydrogen atoms were obtained by riding were refined in a similar manner.

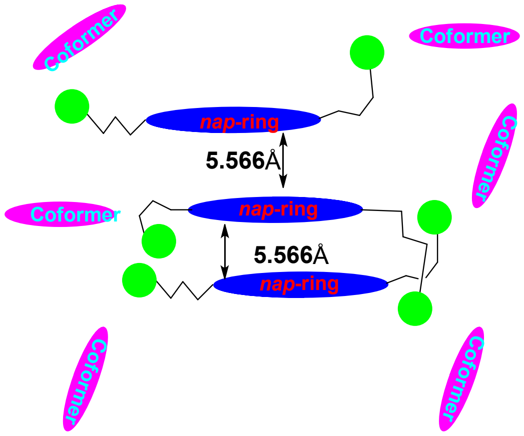

Figure 1S: Centroid to centroid distance of two *nap*-rings in cocrystal **L.cat**, which is not suitable for π-π interactions.

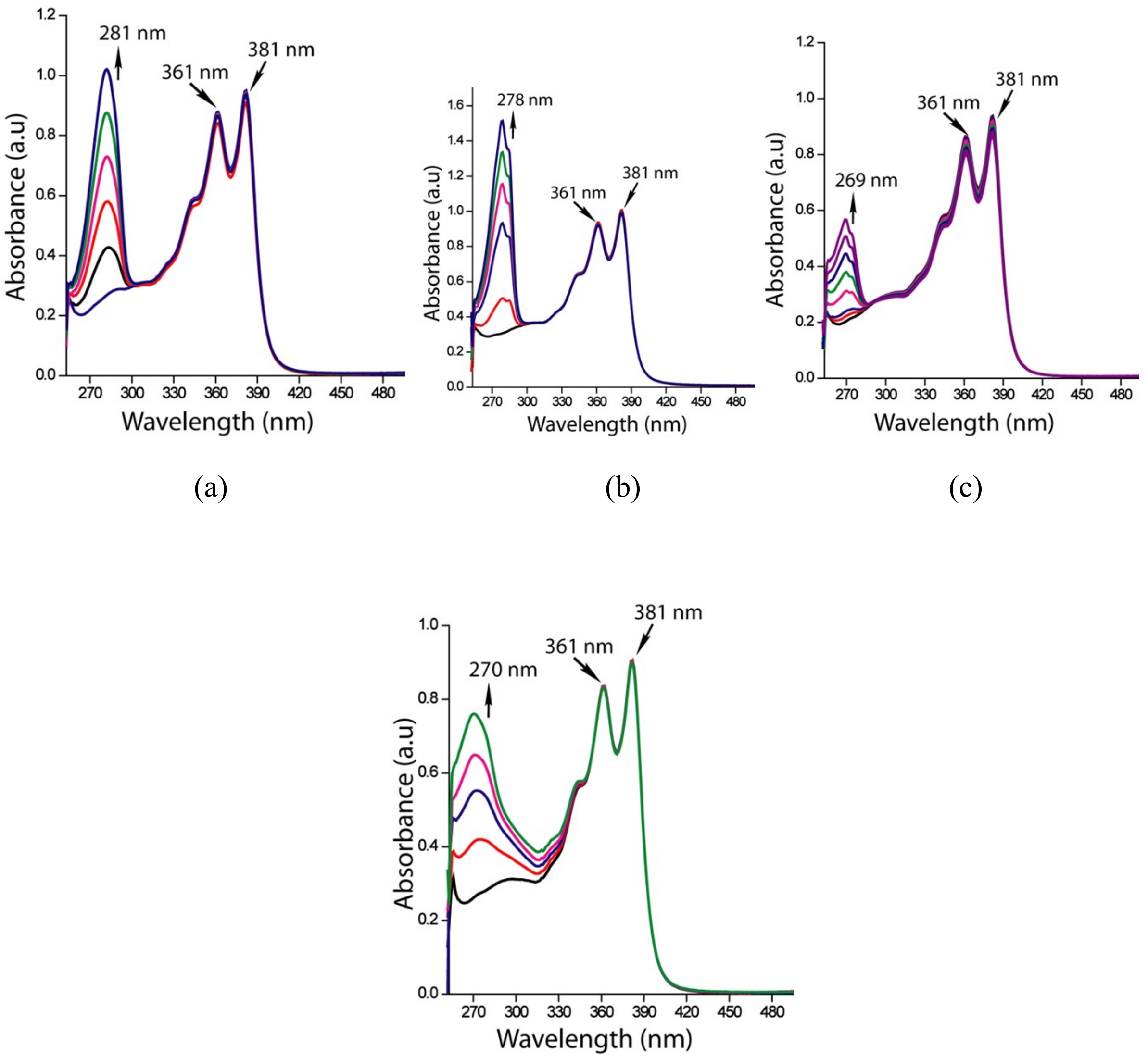

(a) (b) (c)

(d)

Figure 2S: UV-vis spectroscopic titration of **L** (10^{-5}M) with (a) **cat**, (b) **res**, (c) **phi** and (d) **dhpa** of 10^{-4}M methanol solution.

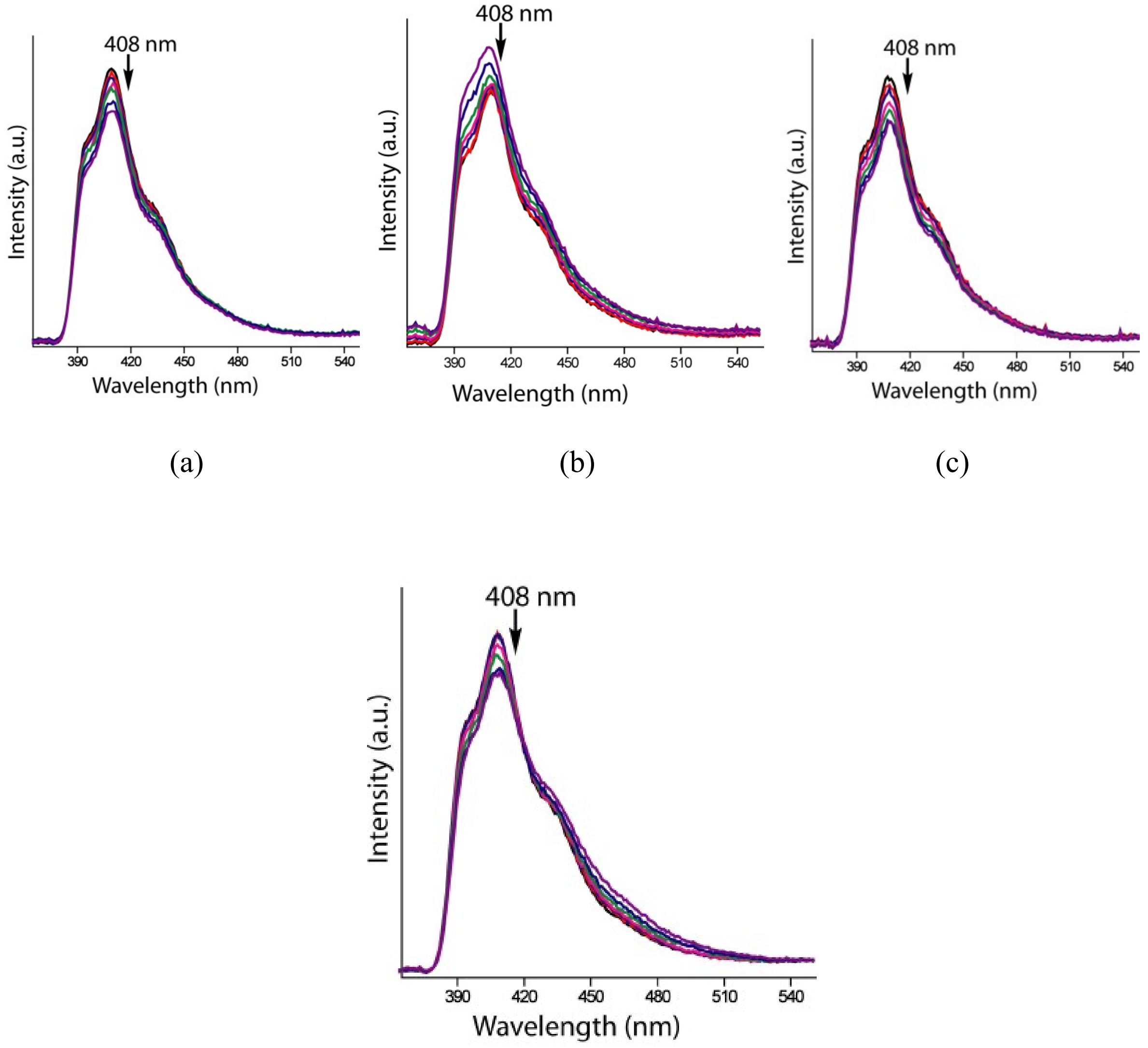

(a)

(b)

(c)

(d)

Figure 3S: Fluorescence emission changes of **L** (10^{-4}M) at 408 nm (excitation at 340 nm) in methanol upon addition of (a) **cat**, (b) **res**, (c) **phi,** and (d) **dhpa** of 10^{-4}M methanol solution.

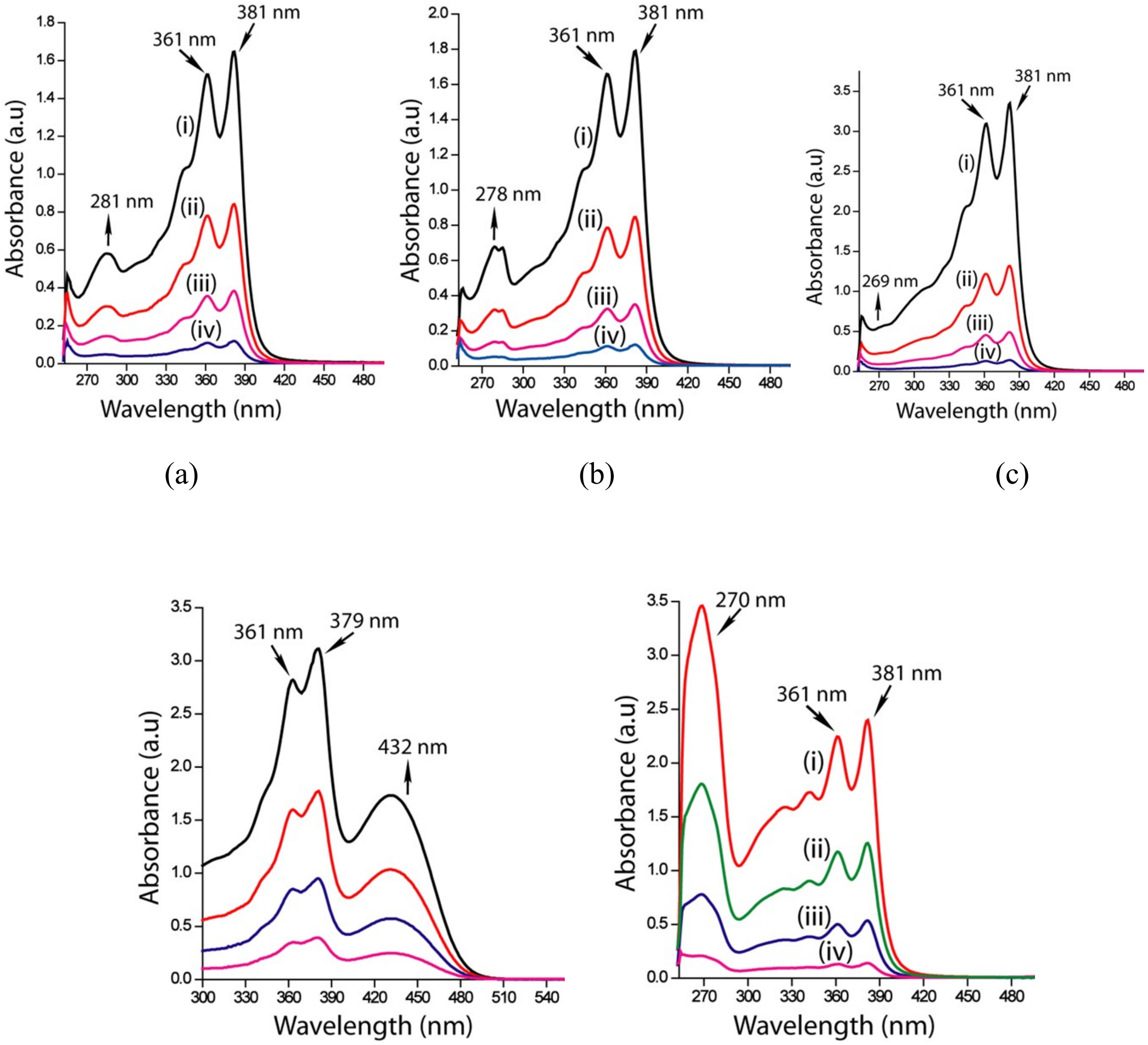

(a) (b) (c)

(d) (e)

Figure 4S: Concentration dependent UV-vis spectra of (a) **L.cat**, (b) **L.(res)$_2$**, (c) **L.phi.H$_2$O,** (d) **L^{2+}.(dnp$^-$)$_2$** and (e) **L.(dhpa)$_2$** in (i) 10^{-4}M, (ii) 10^{-5}M, (iii) 10^{-6}M and (iv) 10^{-7}M methanol solution.

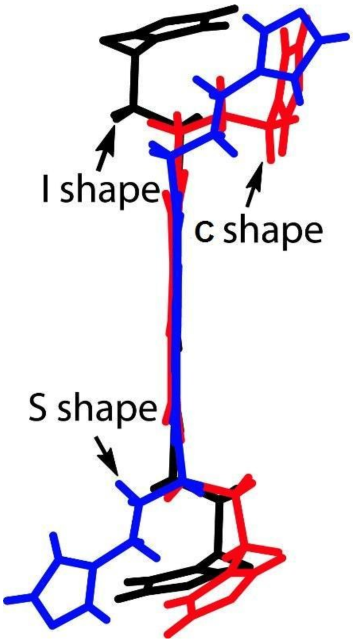

Figure 5S: Overlap diagram of compound **L** in cocrystals **L.(res)$_2$** (blue), **L.(dhpa)$_2$** (black) and **L.phi.H$_2$O** (red).

Table 1S: Different torsion angles of compound **L** in cocrystals and salt.

Compound **L** in cocrystals or salt	Torsion angle (°)	**L.cat**	**L.(res)$_2$**	**L.phi.H$_2$O**	**L^{2+}.(dnp$^-$)$_2$**	**L.(dhpa)$_2$**
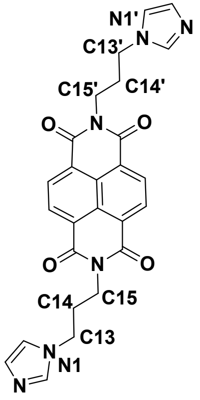	C15-C14-C13-N1	-177.61	177.92	69.23	-68.41	-64.26
	C15'-C14'-C13'-N1'	-57.76	-177.92	-65.10	68.41	64.26

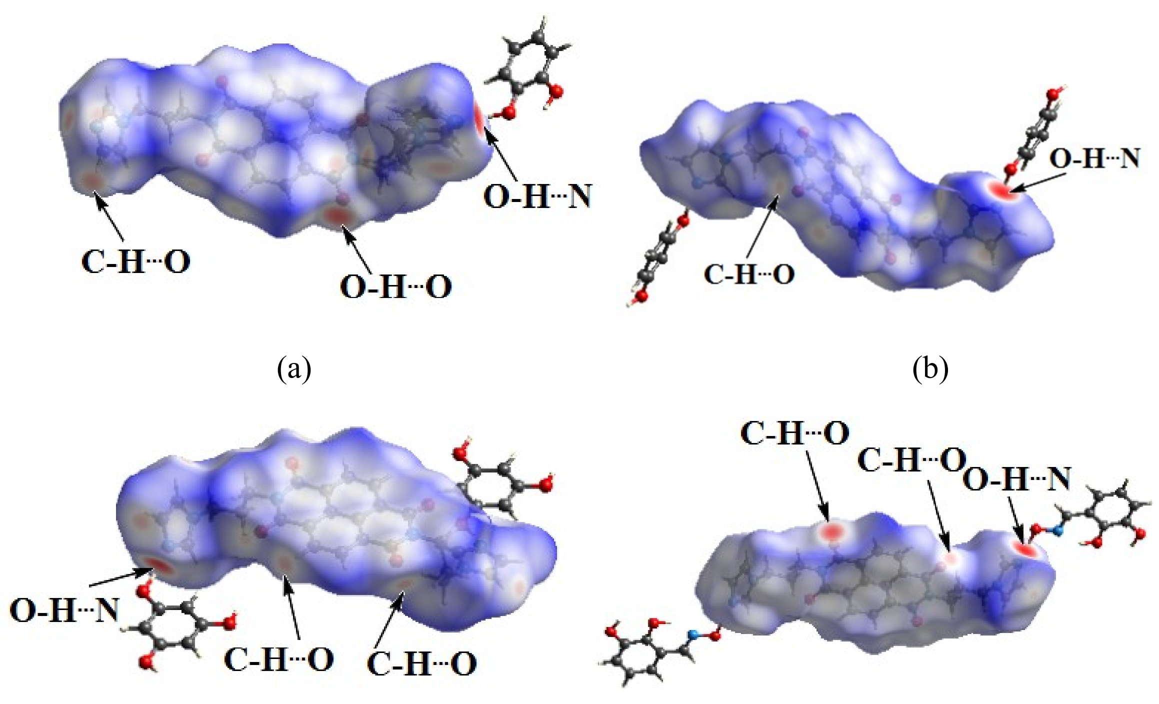

(a) (b)

(c) (d)

Figure 6S: Hirshfeld surface of *nap*-ring segment in (a) **L.cat**, (b) **L.(res)$_2$**, (c) **L.phi.H$_2$O** and (d) **L.(dhpa)$_2$**.

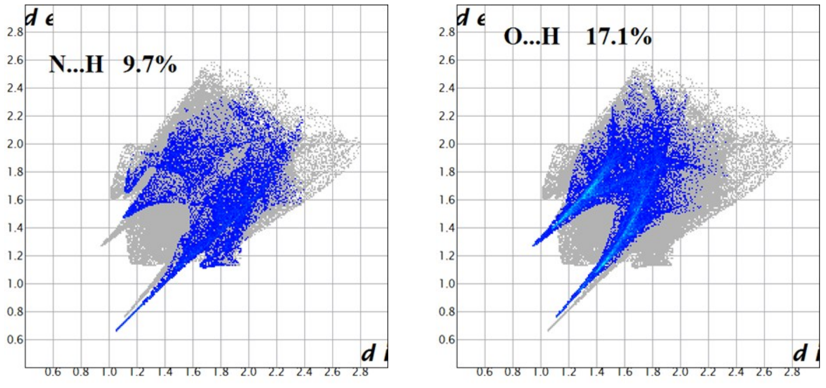

(a)

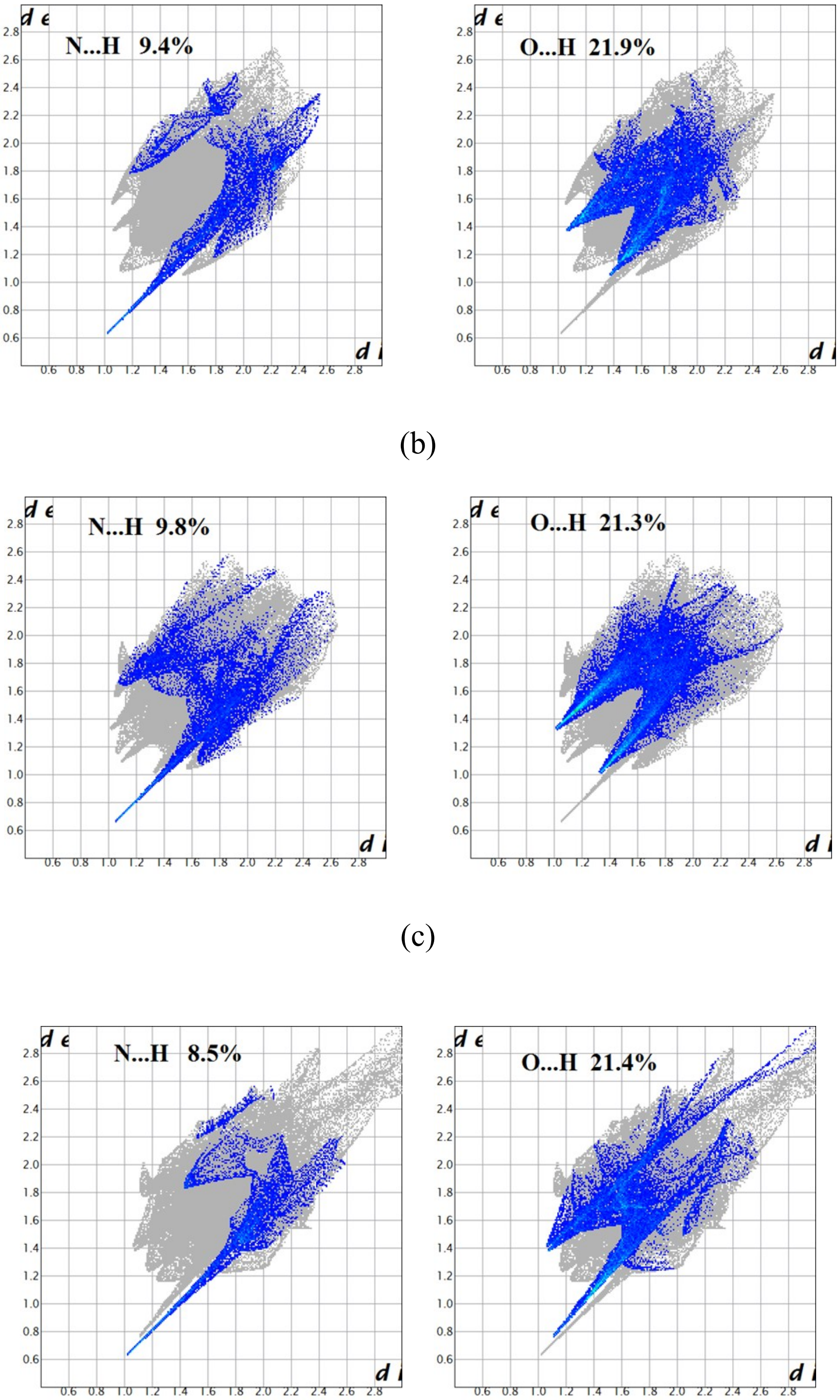

(b)

(c)

(d)

Figure 7S: Fingerprint plots for (a) **L.cat**, (b) **L.(res)$_2$**, (c) **L.phi.H$_2$O** and (d) **L.(dhpa)$_2$** with N···H and O···H interactions highlighted in colour.

Table 2S: Relative contributions of various interactions in percentage to Hirshfeld surface area in cocrystals and salt of **L**.

	L.cat	**L.(res)$_2$**	**L.phi.H$_2$O**	**L.(dhpa)$_2$**	**L^{2+}.(dnp$^-$)$_2$**
O···O	0.9	0.4	1.5	0.6	1.0
N···O	0.4	0.2	1.8	0.5	1.2
C···O	6.4	2.4	2.9	3.0	5.2
H···O	17.1	21.9	21.3	21.4	40.5
C···N	2.2	0.9	0.7	2.6	2.4
N···H	9.7	9.4	9.8	8.5	2.4
C···H	3.2	6.6	6.8	5.2	6.0
C···C	21.4	13.8	14.8	15.8	7.5
H···H	38.4	44.6	40.3	41.8	33.5

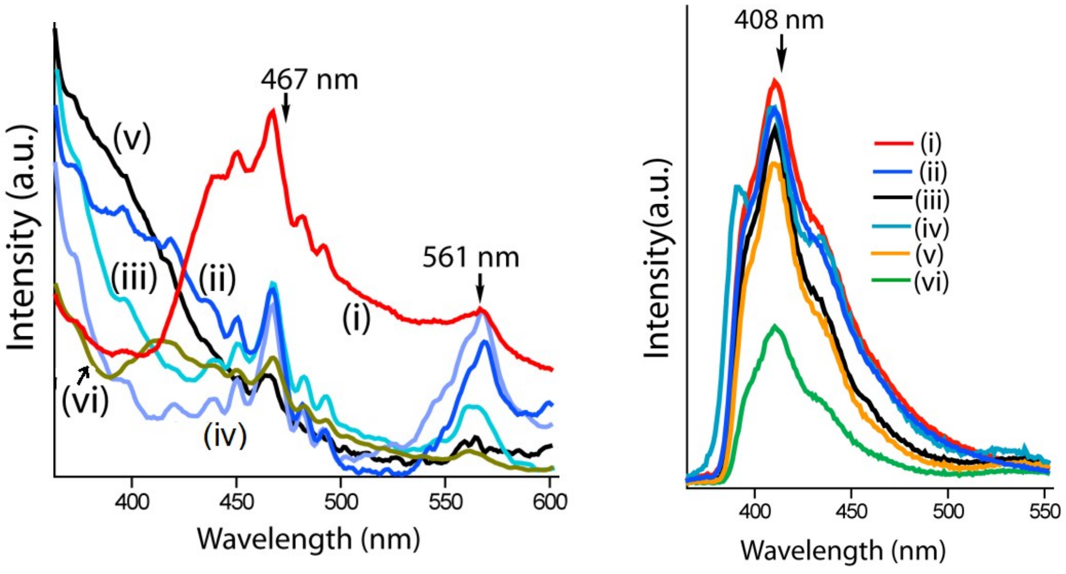

(a) (b)

Figure 8S: Fluorescence emission of (i) **L**, (ii) **L.cat**, (iii) **L.(res)$_2$**, (iv) **L.phi.H$_2$O**, (v) **L.(dhpa)$_2$** and (vi) **L^{2+}.(dnp$^-$)$_2$** in (a) solid-state and (b) in methanol (10^{-4}M).

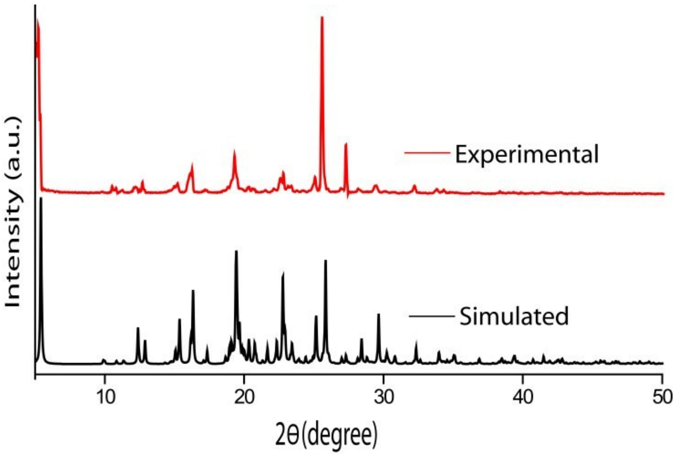

Figure 9S: PXRD patterns of cocrystal **L.cat** (Red= Experimental, Black= Simulated), Simulated pattern generated from CIF file.

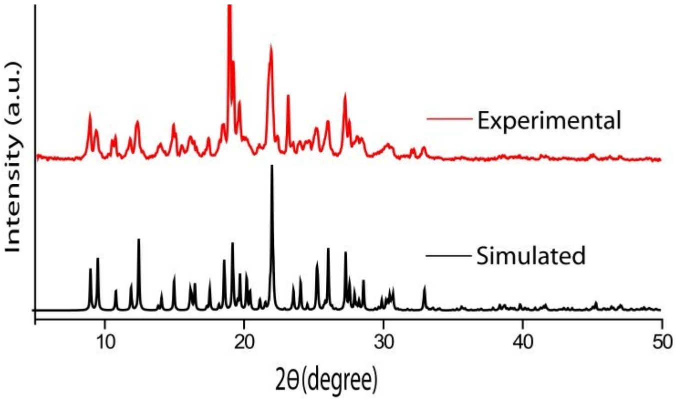

Figure 10S: PXRD patterns of cocrystal **L.(res)$_2$** (Red= Experimental, Black= Simulated), Simulated pattern generated from CIF file.

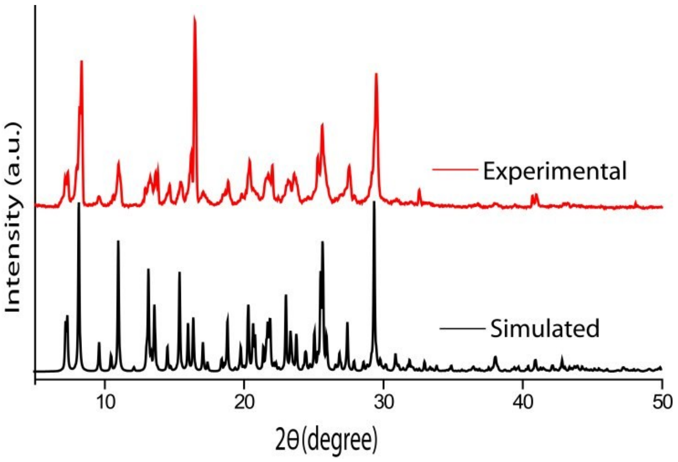

Figure 11S: PXRD patterns of cocrystal **L.phi.H_2O** (Red= Experimental, Black= Simulated), Simulated pattern generated from CIF file.

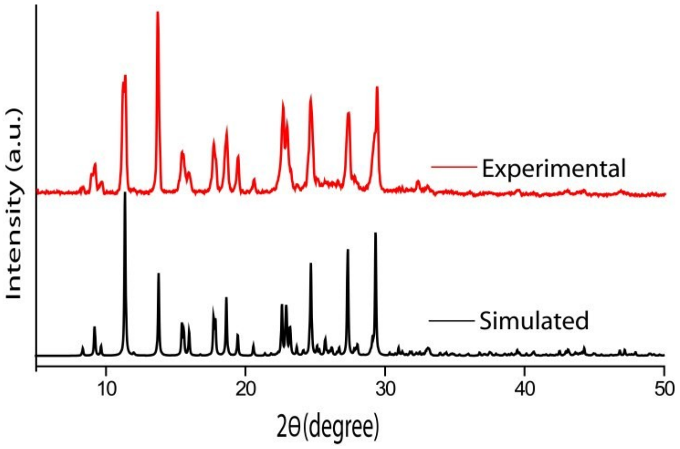

Figure 12S: PXRD patterns of salt **L^{2+}.(dnp$^-$)$_2$** (Red= Experimental, Black= Simulated), Simulated pattern generated from CIF file.

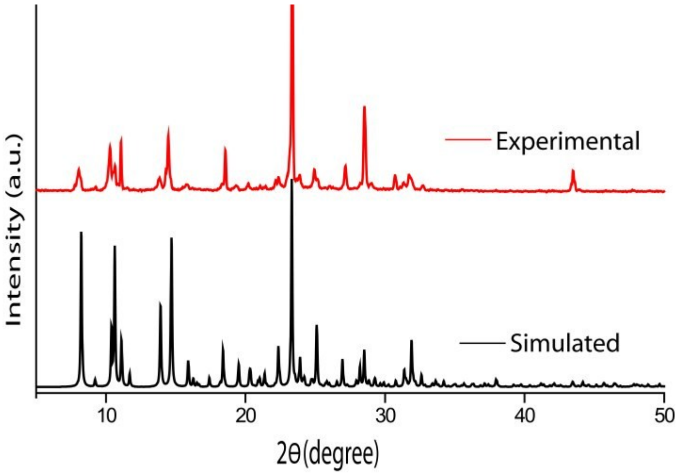

Figure 13S: PXRD patterns of cocrystal **L.(dhpa)$_2$** (Red= Experimental, Black= Simulated), Simulated pattern generated from CIF file.

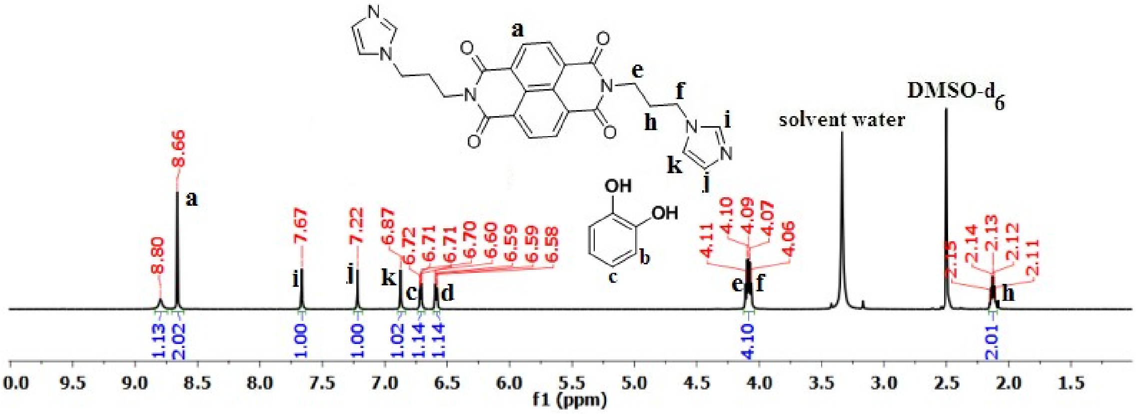

Figure 14S: ^{1}H-NMR (600 MHz, DMSO-d^{6}) spectra of cocrystal **L.cat**.

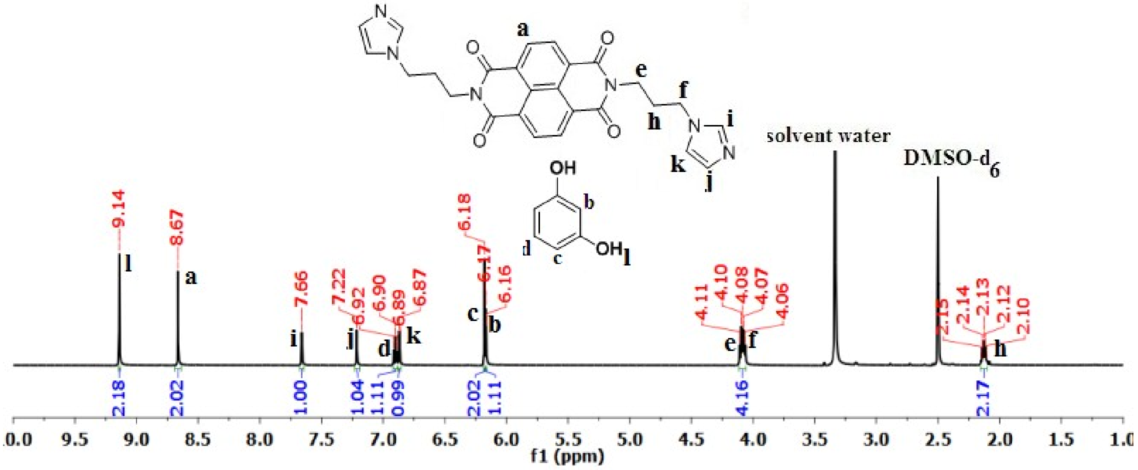

Figure 15S: ^{1}H-NMR (600 MHz, DMSO-d^{6}) spectra of cocrystal **L.(res)$_2$**.

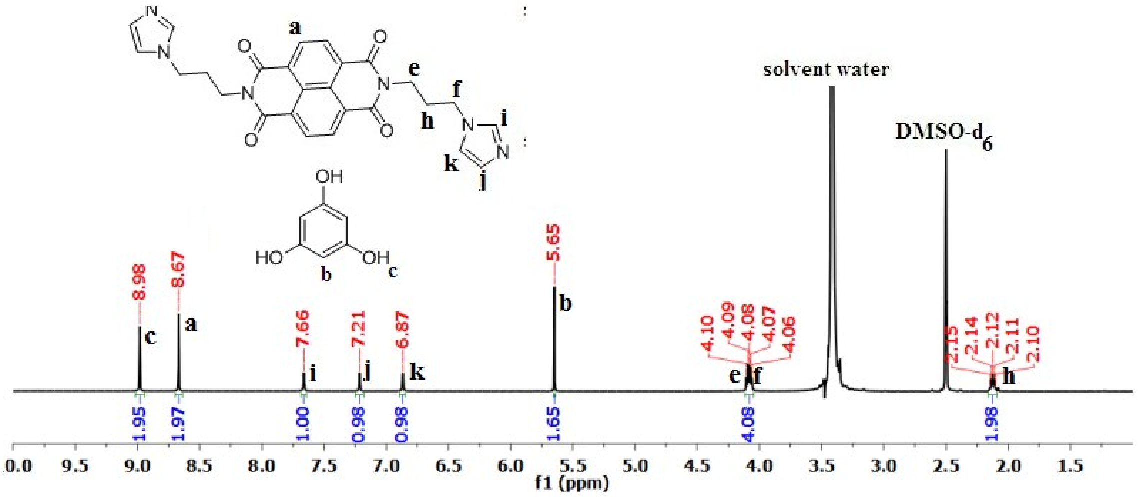

Figure 16S: ^{1}H-NMR (600 MHz, DMSO-d^6) spectra of cocrystal **L.phi.H$_2$O**.

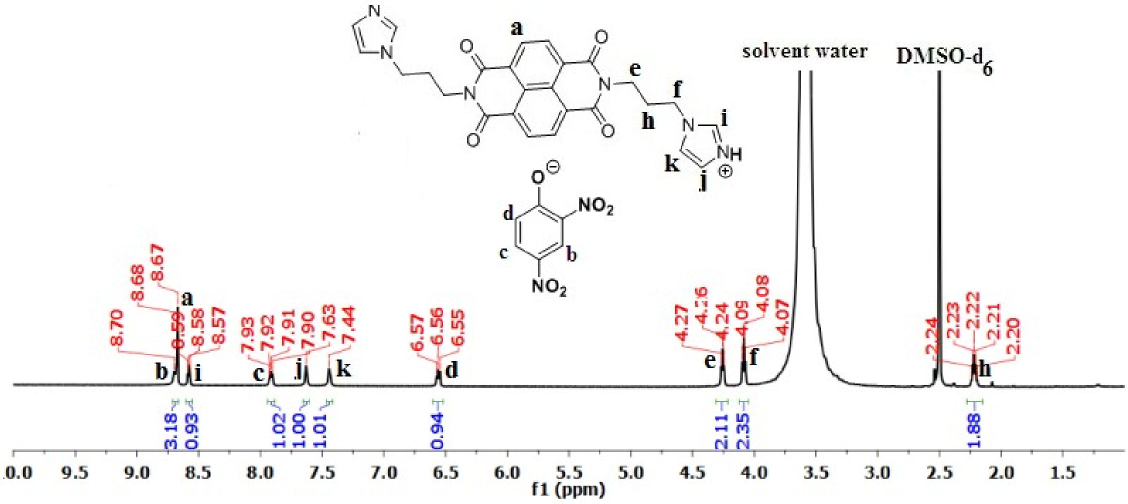

Figure 17S: ^{1}H-NMR (600 MHz, DMSO-d^6) spectra of salt **L^{2+}.(dnp$^-$)$_2$**.

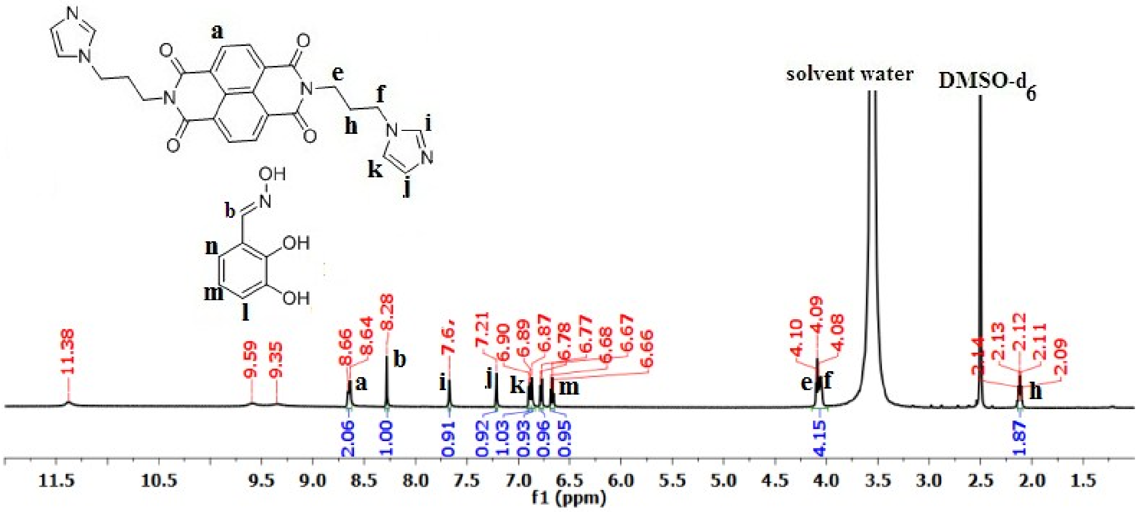

Figure 18S: ^{1}H-NMR (600 MHz, DMSO-d^6) spectra of cocrystal **L.(dhpa)$_2$**.